JFM RAPIDS
journals.cambridge.org/rapids

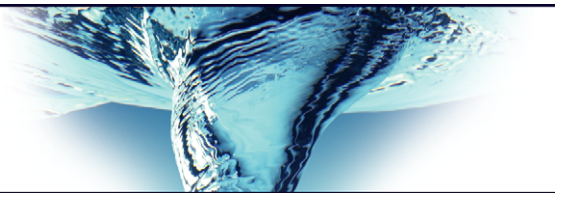

Potential enstrophy in stratified turbulence

Michael L. Waite†

Department of Applied Mathematics, University of Waterloo, 200 University Avenue W., Waterloo, ON N2L 3G1, Canada

(Received 14 December 2012; revised 13 February 2013; accepted 9 March 2013; first published online 9 April 2013)

Direct numerical simulations are used to investigate potential enstrophy in stratified turbulence with small Froude numbers, large Reynolds numbers, and buoyancy Reynolds numbers (Re_b) both smaller and larger than unity. We investigate the conditions under which the potential enstrophy, which is a quartic quantity in the flow variables, can be approximated by its quadratic terms, as is often done in geophysical fluid dynamics. We show that at large scales, the quadratic fraction of the potential enstrophy is determined by Re_b. The quadratic part dominates for small Re_b, i.e. in the viscously coupled regime of stratified turbulence, but not when $Re_b \gtrsim 1$. The breakdown of the quadratic approximation is consistent with the development of Kelvin–Helmholtz instabilities, which are frequently observed to grow on the layerwise structure of stratified turbulence when Re_b is not too small.

Key words: geophysical and geological flows, stratified turbulence, turbulence simulation

1. Introduction

The Ertel potential vorticity (PV) is an important quantity in geophysical fluid dynamics. PV is conserved following the flow in adiabatic rotating stratified fluids, and PV conservation is fundamental to the theory of large-scale quasi-geostrophic (QG) motion in the atmosphere and ocean (e.g. Pedlosky 1987). In this paper, we consider the integrated squared PV, or potential enstrophy, in strongly stratified turbulence without rotation. This parameter regime is relevant at intermediate geophysical scales where QG breaks down. These scales are small enough for Coriolis effects to be weak, but large enough for stratification to be important (i.e. the atmospheric mesoscale and oceanic sub-mesoscale; for a review of stratified turbulence, see Riley & Lelong 2000). PV and potential enstrophy in stratified turbulence are analogous to vorticity and enstrophy in two-dimensional flows, the conservation of which has a profound influence on energy transfers between scales (Fjørtoft 1953). Nevertheless, despite

† Email address for correspondence: mwaite@uwaterloo.ca

doi:10.1017/jfm.2013.150

significant advances in stratified turbulence, the dynamics of potential enstrophy in this regime are not well understood.

Despite the analogy between stratified flows and two-dimensional turbulence, the stratified case is complicated by the fact that PV has linear and quadratic terms in the flow variables. Consequently, potential enstrophy is a quartic, not quadratic, invariant. This structure has curious implications for the evolution of potential enstrophy. For example, viscous effects are not generally restricted to small scales, nor are they purely dissipative; indeed, Herring, Kerr & Rotunno (1994) found viscous generation of potential enstrophy at large scales. However, the quadratic part of the potential enstrophy may dominate under certain conditions, in which case this peculiar behaviour is ruled out. An important example is QG turbulence, which has quadratic potential enstrophy (Charney 1971).

For the case of stratified turbulence, Waite & Bartello (2004) analysed potential enstrophy in the inviscid, truncated equations of motion with strong stratification. By contrast with two-dimensional turbulence, potential enstrophy conservation does not imply an inverse energy cascade. Rather, energy leaks into gravity waves, which are uninhibited by PV conservation and thus can cascade to small scales. Recent simulations by Aluie & Kurien (2011) of strongly stratified, weakly rotating turbulence exhibited a downscale flux of both energy and potential enstrophy. Interestingly, they found the potential enstrophy to be predominantly quadratic in their simulations, and concluded that higher-order terms are relatively small in stratified turbulence. These results are in line with theoretical work by Kurien, Smith & Wingate (2006), who showed that the potential enstrophy is quadratic in the limit of strong stratification and finite viscosity. This finding appears to have important implications for the theory of stratified turbulence, since it implies the existence of an inertial subrange for potential enstrophy, in which the effects of viscosity are restricted to small-scale dissipation.

However, it is not clear whether quadratic potential enstrophy is a generic feature of stratified turbulence. Scale analysis suggests that higher-order terms in the PV are $O(Fr_v^2)$, where $Fr_v \equiv U/(NL_v)$ is the vertical Froude number, U is the horizontal velocity scale, L_v is the vertical length scale, and N is the Brunt–Väisälä frequency (Waite & Bartello 2006). This analysis implies that the potential enstrophy will be quadratic if $Fr_v \ll 1$. But due to the strong anisotropy of stratified turbulence, there is no guarantee of small Fr_v, even if the horizontal Froude number $Fr_h \equiv U/(NL_h)$ is small (L_h is the horizontal length scale). Indeed, scale analysis (Billant & Chomaz 2001) and numerical simulations (Waite & Bartello 2004) indicate that $Fr_v \sim 1$ as $Fr_h \to 0$, provided that viscous effects are sufficiently weak. The tendency for Fr_v to adjust to $O(1)$ has a profound influence on stratified turbulence, which is seen in simulations to have a layerwise 'pancake' structure with layer thickness $L_v \sim U/N$, an energy cascade from large to small horizontal scales, and Kelvin–Helmholtz (KH) instabilities and more isotropic turbulence at smaller scales (e.g. Laval, McWilliams & Dubrulle 2003; Riley & deBruynKops 2003; Lindborg 2006; Waite 2011).

If viscous effects are strong enough, a very different type of stratified turbulence emerges: the layerwise flow becomes viscously coupled and small-scale turbulence is damped (Waite & Bartello 2004). Brethouwer *et al.* (2007) showed that the transition between these regimes depends on the buoyancy Reynolds number $Re_b \equiv Fr_h^2 Re$, where $Re \equiv UL_h/\nu$ is the Reynolds number based on the horizontal scale and ν is the kinematic viscosity. If the kinetic energy (KE) dissipation rate $\epsilon \sim U^3/L_h$, then $Re_b \sim \epsilon/(N^2\nu)$ (e.g. Riley & deBruynKops 2003). If $Fr_h \ll 1$ and $Re_b \gg 1$, stratified turbulence is weakly viscous and $Fr_v \sim 1$; but if $Re_b \ll 1$, stratified turbulence is strongly damped by vertical viscosity. Geophysical stratified turbulence can have

very large Re_b. For example, free-tropospheric mesoscale values of $L_h \sim 100$ km, $U \sim 1$ m s^{-1}, $N \sim 10^{-2}$ s^{-1}, and $\nu \sim 10^{-5}$ m^2 s^{-1} give $Fr_h \sim 10^{-3}$, $Re \sim 10^{10}$, and $Re_b \sim 10^4$. In the stratosphere, typical values of dissipation are $\epsilon \sim 10^{-5}$ m^2 s^{-3} (e.g. Dewan 1997), which gives $Re_b \sim 10^4$. Observations in the ocean thermocline yield $Re_b \sim 10^2$–10^3 (e.g. Moum 1996). By contrast, Re_b can be $O(1)$ or less for laboratory-scale turbulence, due to the smaller Reynolds numbers. For example, $Fr_h \sim 10^{-2}$ and $Re \sim 10^4$ (e.g. Praud, Fincham & Sommeria 2005) give $Re_b \sim 1$.

Given the importance of the buoyancy Reynolds number in stratified turbulence, it is reasonable to suspect that the potential enstrophy dynamics, and in particular the dominance of the quadratic contribution, will depend on Re_b. In this paper, numerical simulations are used to explore the hypothesis that the potential enstrophy will be approximately quadratic only for $Re_b \ll 1$. Equations and parameter regimes are reviewed in § 2, and the computational methodology is described in § 3. Results are presented in § 4, in which the quadratic and higher-order contributions to the potential enstrophy are examined at different Fr_h and Re_b. Discussion and conclusions are given in § 5.

2. Governing equations and parameter regimes

We consider stratified turbulence governed by the Boussinesq equations

$$\mathrm{D}_t \boldsymbol{u} + f\hat{\boldsymbol{z}} \times \boldsymbol{u} = -\boldsymbol{\nabla} p + b\hat{\boldsymbol{z}} + \nu \nabla^2 \boldsymbol{u} + \boldsymbol{F}, \quad \boldsymbol{\nabla} \cdot \boldsymbol{u} = 0, \tag{2.1}$$

$$\mathrm{D}_t b + N^2 w = \kappa \nabla^2 b, \tag{2.2}$$

where $\mathrm{D}_t \equiv \partial_t + \boldsymbol{u} \cdot \nabla$ is the material derivative, $\boldsymbol{u}$ is the velocity, w is the vertical velocity component, $\hat{\boldsymbol{z}}$ is the vertical unit vector, b is the buoyancy, p is the pressure scaled by a reference density, f is the Coriolis parameter, κ is the mass diffusivity, and $\boldsymbol{F}$ is forcing. In what follows, we will assume $\kappa = \nu$ and constant N.

Stratified turbulence requires $Fr_h \ll 1$ and $Re \gg 1$. However, due to the anisotropic pancake structures that emerges at strong stratification, the threshold for 'large' Re depends on Fr_h. Brethouwer *et al.* (2007) framed this condition in terms of the buoyancy Reynolds number: weakly viscous stratified turbulence requires $Fr_h \ll 1$ and $Re_b \gg 1$, i.e. Re must be large compared to Fr_h^{-2} as $Fr_h \to 0$. Lindborg (2006) proposed a direct energy cascade theory for this regime, with horizontal and vertical wavenumber KE spectra of $k_h^{-5/3}$ and k_v^{-3}, respectively. Numerical simulations have been broadly consistent with this picture, though a range of spectral slopes have been observed (e.g. Riley & deBruynKops 2003; Waite & Bartello 2004; Brethouwer *et al.* 2007; Almalkie & deBruynKops 2012; Kimura & Herring 2012). In addition, the emergence of KH instabilities at small scales yields bumps in the k_h spectra and a transition to small-scale three-dimensional turbulence (Laval *et al.* 2003; Waite 2011). By contrast, for $Re_b \ll 1$, the Lindborg (2006) cascade and KH instabilities are suppressed, the horizontal energy spectrum steepens to k_h^{-5}, and the vertical spectrum is flat out to the dissipation range, which is consistent with layerwise flow coupled only by viscosity (Waite & Bartello 2004; Brethouwer *et al.* 2007).

The vertical Froude number in stratified turbulence depends on the value of Re_b. For large Re_b, L_v scales like the buoyancy scale $L_b \equiv U/N$ and $Fr_v \sim 1$ (as predicted by Billant & Chomaz 2001 and demonstrated numerically by Waite & Bartello 2004). However, for small Re_b, L_v scales like the viscous scale $L_{visc} \equiv \sqrt{\nu L_h / U}$ (e.g. Riley & deBruynKops 2003; Godoy-Diana, Chomaz & Billant 2004; Brethouwer *et al.* 2007), and thus $Fr_v \sim \sqrt{Re_b}$. As a result, small Fr_v values are only expected in the viscously coupled regime of $Re_b \ll 1$, where the vertical scale is limited by viscosity. Even at

apparently large Reynolds numbers, this regime can always be obtained by increasing the stratification at fixed Re. Analogously, in simulations with numerical or ad hoc viscosity (e.g. hyperviscosity, eddy viscosity), the viscously coupled regime will ultimately be reached by increasing the stratification at fixed numerical resolution (as in e.g. Waite & Bartello 2004).

The Ertel PV for (2.1)–(2.2) is

$$\Pi \equiv (\boldsymbol{\omega} + f\hat{\boldsymbol{z}}) \cdot (N^2\hat{\boldsymbol{z}} + \boldsymbol{\nabla} b) = fN^2 + (N^2\omega_z + f\partial_z b) + \boldsymbol{\omega} \cdot \boldsymbol{\nabla} b, \tag{2.3}$$

where $\boldsymbol{\omega} \equiv \nabla \times \boldsymbol{u}$. The terms on the right-hand side of (2.3) are denoted Π_0, Π_1, and Π_2, respectively, where the subscript gives the order in the variables $\boldsymbol{\omega}$ and b. The constant term Π_0 is trivially conserved and can be neglected. The evolution equation for Π is

$$\mathrm{D}_t \Pi = (N^2\hat{\boldsymbol{z}} + \boldsymbol{\nabla} b) \cdot (\nu\nabla^2\boldsymbol{\omega} + \boldsymbol{\nabla} \times \boldsymbol{F}) + \kappa(f\hat{\boldsymbol{z}} + \boldsymbol{\omega}) \cdot \boldsymbol{\nabla}(\nabla^2 b), \tag{2.4}$$

which makes it clear that Π is conserved following the flow in the absence of viscosity, diffusion, and forcing. The potential enstrophy is given by

$$V \equiv \tfrac{1}{2}\langle \Pi^2 \rangle \equiv \tfrac{1}{2}\langle \Pi_1^2 \rangle + \langle \Pi_1 \Pi_2 \rangle + \tfrac{1}{2}\langle \Pi_2^2 \rangle, \tag{2.5}$$

where $\langle \cdot \rangle$ means spatial average. We denote the terms on the right-hand side of (2.5) by V_2, V_3, and V_4, respectively, which correspond to the quadratic, cubic, and quartic contributions to the potential enstrophy.

Following Waite & Bartello (2006), we can use scale analysis to estimate the relative size of Π_1 and Π_2. Making the standard assumptions of $L_v/L_h \lesssim 1$ and $b \sim U^2/L_v$ (e.g. Riley & Lelong 2000), we obtain

$$\Pi_1 \sim N^2 U/L_h \max(1, Fr_v^2/Ro), \quad \Pi_2 \sim U^3/(L_h L_v^2), \tag{2.6}$$

where $Ro \equiv U/(f\,L_h)$ is the Rossby number. These estimates are of the dominant scale; some terms in Π_2 may be smaller (Billant & Chomaz 2001). For flows strongly affected by rotation, $\Pi_2/\Pi_1 \lesssim Ro \ll 1$, and the PV is approximately quadratic. However, a different balance emerges when $Ro \gtrsim Fr_v^2$, which is the case in stratified turbulence with weak or no rotation, as in the atmospheric mesoscale and oceanic sub-mesoscale. In this regime, the ratio of the quadratic and linear parts of the PV is $\Pi_2/\Pi_1 \sim Fr_v^2$. As a result, Π_1 will dominate over Π_2 – and, consequently, the quadratic potential enstrophy will dominate over the cubic and quartic contributions – when $Fr_v \ll 1$. But small vertical Froude numbers are only expected for small Re_b. For larger Re_b, which is the more geophysically relevant parameter regime, this scale analysis suggests that $V_2 \sim V_3 \sim V_4$.

3. Numerical approach

To explore how the different terms in the potential enstrophy vary with Re_b, we have performed direct numerical simulations (DNS) of forced stratified turbulence with small Froude number ($Fr_h \lesssim 0.02$) and large Reynolds number ($Re \gtrsim 4000$). Simulations are configured to have similar values of U and L_h, so the Froude and Reynolds numbers are varied by changing N and ν. Four stratifications and two viscosities are considered to yield a range of buoyancy Reynolds numbers on both sides of unity ($0.002 \lesssim Re_b \lesssim 4$; simulation parameters are given in table 1). The Coriolis parameter f is set to zero.

The governing equations are solved numerically in a triply periodic domain of size $L^3 = (2\pi)^3$. The numerical model employs a Fourier-based spectral method,

Run	n	N	ν	Fr_h	Re	Re_b
A1	512	0.283	0.125×10^{-4}	0.022	3800	1.8
A2	512	0.566	0.125×10^{-4}	0.010	4800	0.48
A3	512	1.13	0.125×10^{-4}	0.0043	7200	0.13
A4	512	10	0.125×10^{-4}	0.00046	9700	0.0020
B1	960	0.283	0.0625×10^{-4}	0.021	8300	3.6
B2	960	0.566	0.0625×10^{-4}	0.010	9000	0.94
B3	960	1.13	0.0625×10^{-4}	0.0045	13000	0.26
B4	960	10	0.0625×10^{-4}	0.00044	22000	0.0041
A1r	960	0.283	0.125×10^{-4}	0.021	4000	1.8

TABLE 1. Summary of simulations. In the labels, letter (A, B) denotes viscosity and number (1–4) denotes stratification. Run A1r is a high-resolution version of A1.

with third-order Adams–Bashforth time stepping for the advection, buoyancy, and forcing terms. Viscous terms are treated implicitly using a trapezoidal approach. The spatial resolution is uniform in the horizontal and vertical, with n wavenumbers and grid points in each direction. Aliasing errors are removed by truncating the Fourier coefficients with the 2/3 rule after computing convolutions in physical space, i.e. by keeping only wavevectors $\boldsymbol{k}$ with $k \equiv |\boldsymbol{k}| \leqslant k_T \equiv n/3$. As a result, the effective grid spacing is $\Delta x \equiv 1.5L/n$. Two resolutions are employed: $n = 512$ and 960 for the larger and smaller ν, respectively. These are chosen to resolve the Kolmogorov wavenumber with $k_T/k_d \approx 1$, where $k_d \equiv (\epsilon/\nu^3)^{1/4}$. One additional high-resolution simulation with $k_T/k_d \approx 2$ was also performed (run A1r in table 1).

Statistically stationary turbulence is maintained with a random velocity forcing $\boldsymbol{F}$ (e.g. Kimura & Herring 2012). Following Aluie & Kurien (2011), forcing is restricted to wave vectors in a spherical shell centred on $k_f = 4$. The forcing is horizontally non-divergent in order to excite only vortical modes, which account for the linear part of the PV (Bartello 1995). Such vortical forcing is commonly used in numerical studies of stratified turbulence to avoid complications from large-amplitude, large-scale internal waves (e.g. Waite & Bartello 2004; Lindborg 2006; Kimura & Herring 2012). Note, however, that Aluie & Kurien (2011) forced vortical modes and internal waves. The amplitude of the forcing is set to give $\epsilon \approx 2 \times 10^{-6}$, which yields a forcing time scale of around $\tau_f \equiv \epsilon^{-1/3} k_f^{-2/3} \approx 30$. Vertically sheared uniform flow with $k_h = 0$ is damped with a weak linear drag (time scale of 1000) to avoid the slow growth of these modes (Smith & Waleffe 2002).

For the larger-ν simulations, the velocity and buoyancy fields are initialized with low-level noise and run for 2000 time units, with various quantities (ϵ, V, etc.) averaged over $1000 \leqslant t \leqslant 2000$. The length of the averaging interval corresponds to $\approx 30\tau_f$. Simulations with smaller ν are initialized with the larger-ν fields at $t = 1000$ and averaged over $1200 \leqslant t \leqslant 2000$. To compute the Froude and Reynolds numbers, U is defined as the root-mean-square velocity and L_h is obtained from the average dissipation rate using $L_h \equiv U^3/\epsilon$. As a result, the velocity and length scales are flow-dependent and vary slightly from simulation to simulation; however, they are around $U \approx 0.02$ and $L_h \approx 4$ in all cases. It is also possible to define a forcing-based Froude

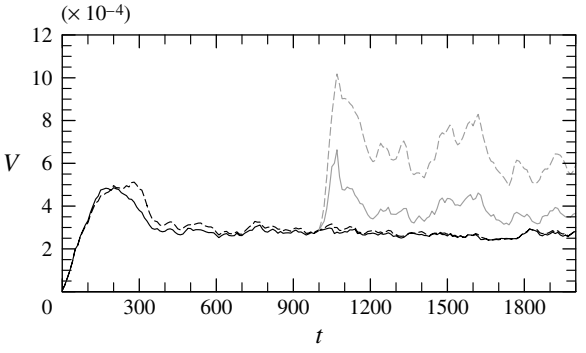

FIGURE 1. Time series of V (solid) and V_2 (dashed) for $Fr_h = 0.01$ with $Re_b = 0.48$ (black) and $Re_b = 0.94$ (grey) (runs A2 and B2, respectively).

number $Fr_f \equiv 1/(N\tau_f)$ (as in Aluie & Kurien 2011). Our strongest stratification $N = 10$ was chosen to yield $Fr_f = 0.003$, which is close to (in fact, slightly larger than) the stratified turbulence simulation in Aluie & Kurien (2011), which has $Fr_f = 0.002$.

4. Results

Time series of the total and quadratic potential enstrophy are shown in figure 1 for the two simulations with $Fr_h = 0.01$ ($Re_b = 0.48$ and 0.94). The lower-Re_b case starts at $t = 0$ and takes several hundred time units to adjust to the forcing; the time series appear to be statistically stationary by around $t \approx 500$. The potential enstrophy is nearly quadratic in this simulation, with V_2 only slightly different (in fact, larger) than V. Since V_4 is positive definite, the implication is that the cubic term $V_3 < 0$. At $t = 1000$, the higher-resolution simulation with $Re_b = 0.94$ is started. Both V and V_2 increase rapidly in response to the change in Re_b, after which V_2 remains significantly larger, by around 70 %, than V. Figure 1 makes it clear that the relative importance of the quadratic potential enstrophy is not simply a function of Fr_h, since both experiments have $Fr_h = 0.01$. Increasing Re_b at fixed stratification appears to make the higher-order contributions to V more significant.

This dependence on Re_b holds at other stratifications as well. The quadratic and quartic fractions of the potential enstrophy V_2/V and V_4/V are shown in figure 2 for all simulations. For sufficiently small Fr_h (figure 2*a*), the potential enstrophy is predominantly quadratic. As the Froude number is increased to $Fr_h \approx 0.01$–0.02, which is still small enough for stratified turbulence, higher-order contributions become important. At these stratifications the quadratic potential enstrophy is larger than V by around a factor of two, and the quartic term V_4 has the same order of magnitude as V_2 (as does the cubic term V_3, which is negative). However, as suggested by the time series in figure 1, these ratios are not simply functions of Fr_h. Decreasing Re at fixed Fr_h, i.e. going from the grey to black curves in figure 2(*a*), leads to a significant decrease in the quartic contribution V_4/V at all Fr_h.

Some of the joint dependence of these ratios on Fr_h and Re can be accounted for by a dependence on Re_b (figure 2*b*). For relatively small $Re_b < 0.4$, i.e. in the viscously coupled layerwise regime of stratified turbulence, the potential enstrophy is essentially quadratic, with the small quartic contribution collapsing onto a single function of Re_b. The ratio V_4/V appears to go to zero as $Re_b \to 0$. However, for larger

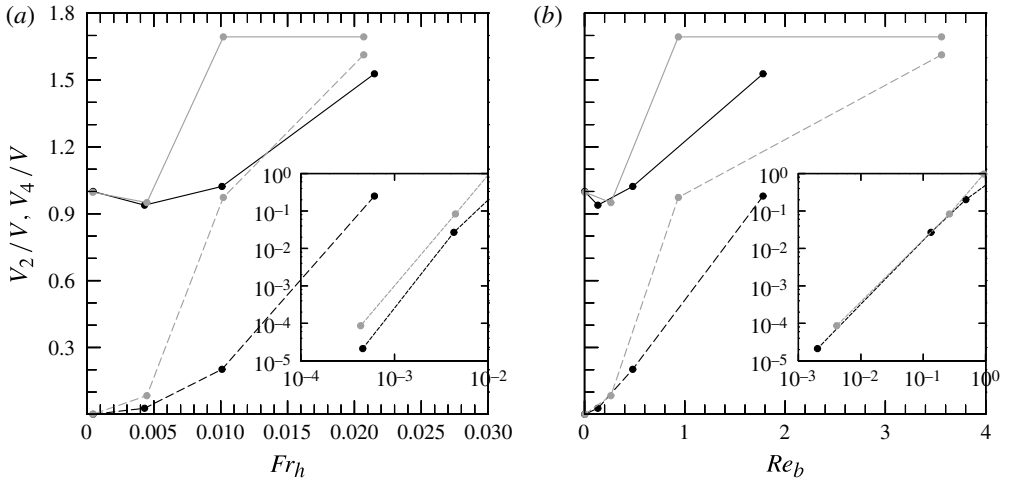

FIGURE 2. Fraction of time-averaged quadratic (solid) and quartic (dashed) contributions to the potential enstrophy (V_2/V and V_4/V, respectively), plotted against (*a*) Fr_h and (*b*) Re_b. Simulations with $\nu = 0.125 \times 10^{-4}$ are black, and with $\nu = 0.0625 \times 10^{-4}$ are grey. The quartic contributions at small Fr_h and Re_b are shown with log–log axes in the insets.

$Re_b \sim 1$, the collapse with respect to Re_b fails, and the contribution from the quartic term is significant; indeed, it has the same order of magnitude as V_2 and V itself. The quadratic contribution is therefore a poor approximation to the full potential enstrophy in this regime, which corresponds to the transition from viscous layering to weakly viscous stratified turbulence.

Horizontal wavenumber spectra can provide insight into the dependence of the terms in the potential enstrophy on Re_b. Spectra of V, V_2 and V_4 are plotted in figure 3 for simulations with $Fr_h = 0.02$, 0.01 and 0.004, for which the higher-order terms in V make the largest contributions. These spectra are computed from Π_1 and Π_2 by integrating the modal PV variances over cylindrical wavenumber shells in the usual way (e.g. Waite & Bartello 2004; Kimura & Herring 2012); they give the contribution to the potential enstrophy from different horizontal length scales. Note that the V spectra exhibit a bulge at the very largest wavenumbers ($k_h \approx 100$ and 200 in figures 3*a,c* and 3*b,d,f*, respectively). This bulge is an artifact of the wavenumber truncation in these simulations, and is more pronounced in the higher-order contributions to the potential enstrophy. We have verified that this bulge moves downscale when higher resolution is employed (see grey curves in figure 3*a*, which were computed with $n = 960$). Apart from this feature at very small scales, the V spectra are well-resolved and robust to increased resolution.

The potential enstrophy spectra are peaked at large horizontal scales ($2 \leqslant k_h \leqslant 4$), consistent with the vortical mode forcing around $k = 4$. V is mostly quadratic at these scales, and increasingly so as Fr_h is reduced. In contrast to the totals plotted in figure 2, the large-scale V_2 is smaller than V. The combined contribution from V_3 and V_4 at large scales is therefore small and positive. However, the situation changes dramatically as one moves to smaller horizontal scales. The V_2 spectra have a pronounced bump at intermediate k_h (e.g. around $k_h \approx 20$ in figure 3*a*), which is not present in the V spectra. Unlike the bulge at the largest k_h described above, this intermediate-k_h bump is robust and well-resolved (figure 3*a*). It is because of this

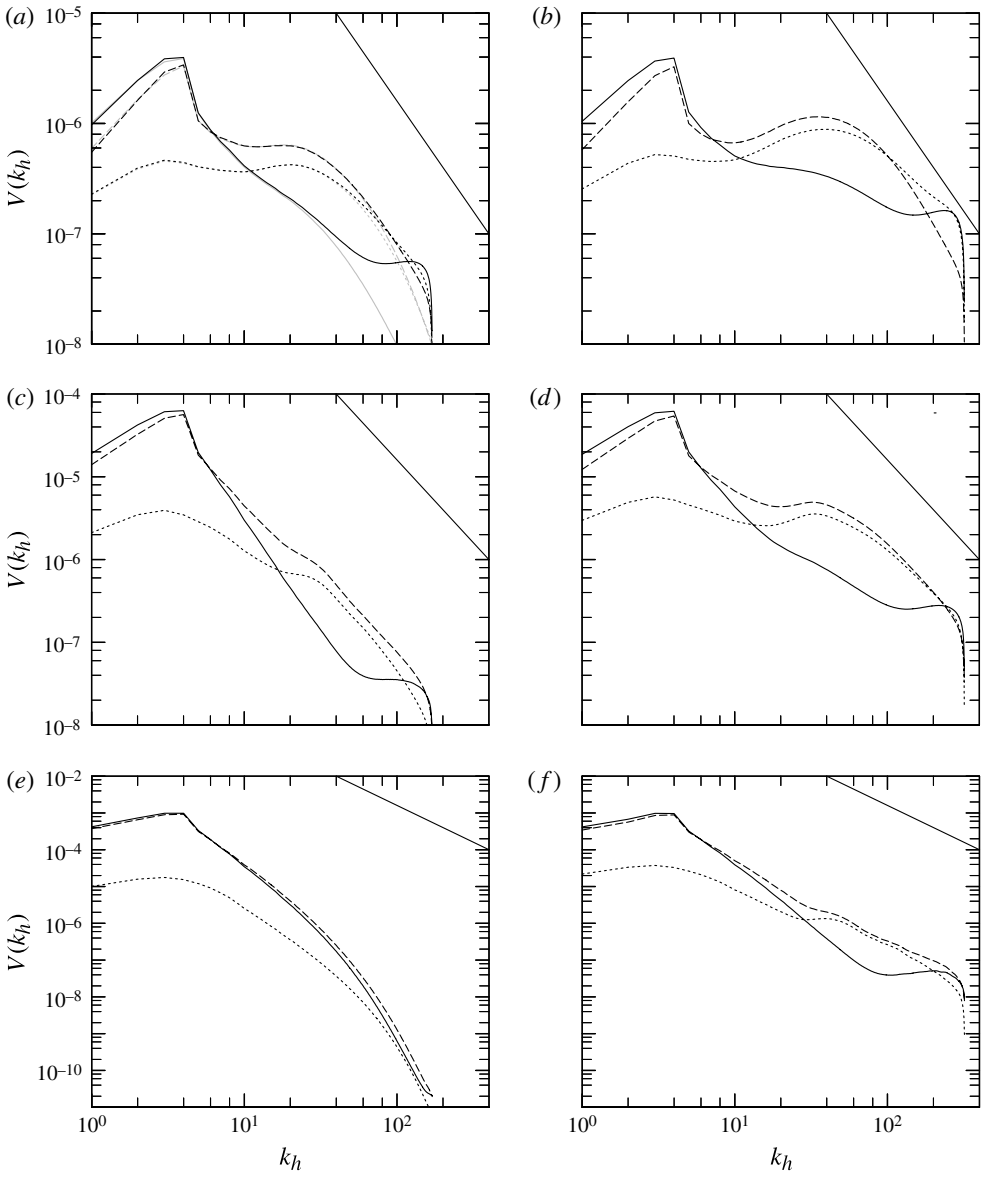

FIGURE 3. Time-averaged horizontal wavenumber spectra of V (solid), V_2 (long dashed), and V_4 (short dashed). Top plots have $Fr_h = 0.02$ and $Re_b =$ (*a*) 1.8 and (*b*) 3.6; middle plots have $Fr_h = 0.01$ and $Re_b =$ (*c*) 0.48 and (*d*) 0.94; and bottom plots have $Fr_h = 0.004$ and $Re_b =$ (*e*) 0.13 and (*f*) 0.26 (runs A1, B1, A2, B2, A3 and B3, respectively). In (*a*), a high-resolution test (run A1r) is shown in grey. The reference line has slope -2.

bump that the total domain-averaged V_2 over-estimates V in figure 2. The bump is diminished when Re_b decreases, either by decreasing Fr_h (compare upper and lower plots in figure 3 or by decreasing Re (compare right and left plots in figure 3. In fact, the bump disappears completely for $Re_b = 0.13$ (figure 3*e*) as well as smaller Re_b (runs A4 and B4, not shown).The V_4 spectra are similarly peaked at intermediate scales, as

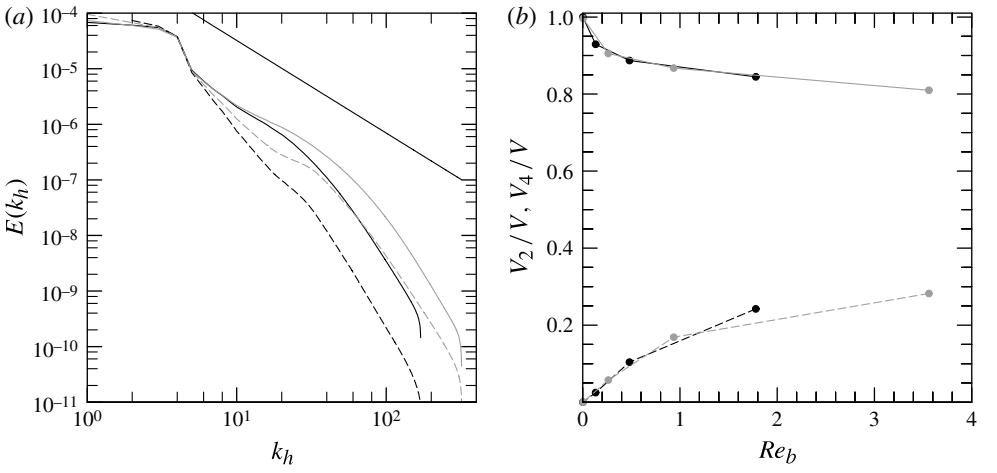

FIGURE 4. (*a*) Time-averaged horizontal wavenumber spectra of KE for $Fr_h = 0.02$ (solid) and 0.01 (dashed), for lower (black) and higher (grey) Re_b (runs A1, A2, B1 and B2, respectively), along with a reference slope of $-5/3$. (*b*) Fraction of time-averaged large-scale quadratic (solid) and quartic (dashed) contributions to V (as in figure 2*b*, but enstrophy is restricted to $k_h \leqslant 10$). Simulations with $\nu = 0.125 \times 10^{-4}$ are black, and with $\nu = 0.0625 \times 10^{-4}$ are grey.

is V_3, which has a negative bump (implied by figure 3, since $V_3 = V - V_2 - V_4$). When summed together, these bumps cancel out, yielding V spectra that are much steeper than those of V_2, V_3 and V_4.

The V_2 spectrum is proportional to the vortical KE spectrum multiplied by k_h^2 (Bartello 1995). As a result, shallowing of the KE spectra to a $-5/3$ power law, which is expected for large Re_b, should yield V_2 spectra with positive slopes out to the dissipation range, as in figure 3. However, the bumps in the V_2 spectra are also reminiscent of bumps in the energy spectra (figure 4*a*), which have been attributed in previous studies to KH instabilities of the layerwise flow (Laval *et al.* 2003; Brethouwer *et al.* 2007; Waite 2011). As these instabilities evolve at finite amplitude and roll up into KH billows, they inject energy into horizontal scales on the order of the billow size, which is expected to be similar to the layer thickness. Waite (2011) showed that these bumps appear at horizontal scales around L_b in simulations with hyperviscosity (i.e. effectively large Re_b). More recently, Waite (2013) showed that they can also appear at the viscous scale in DNS with $Re_b \sim 1$. The bumps in the V_2 spectra in figure 3 are consistent with this interpretation.

The bumps in figure 3 are responsible for the behaviour observed in figure 2(*b*), in which the ratios V_2/V and V_4/V were found to not collapse when plotted against Re_b for $Re_b \sim 1$. Depending on the value of Re_b, the layer thickness in stratified turbulence, and hence the scale of the KH instabilities, is either L_b or L_{visc} (e.g. Hebert & deBruynKops 2006; Brethouwer *et al.* 2007; Waite 2011, 2013). But neither of these scales is determined by Re_b alone, since $L_b/L_h \sim \sqrt{Re_b/Re}$ and $L_{visc}/L_h \sim 1/\sqrt{Re}$. As a result, there is no reason to expect the higher-order contributions to the potential enstrophy from these scales to depend solely on Re_b. We can remove the contribution from the bumps by computing V, V_2, and V_4 from large horizontal scales only ($k_h \leqslant 10$). These ratios are plotted in figure 4(*b*), and the collapse with respect to Re_b is excellent.

5. Conclusions

We have shown that the quadratic part of the potential enstrophy is not a good approximation to the total when $Re_b \gtrsim 1$, even in strongly stratified turbulence with $Fr_h \ll 1$. The parameter regime of $Re_b \gtrsim 1$ corresponds to marginally or weakly viscous stratified turbulence, which is characterized by layerwise flow with associated KH instabilities and (for $Re_b \gg 1$) more isotropic three-dimensional turbulence at small scales. The breakdown of the quadratic approximation appears to occur at intermediate horizontal scales, where bumps in the KE spectra suggest the growth of KH billows (as in Laval *et al.* 2003 and Waite 2011; the same process has been reported in the breakdown of a vortex dipole by Augier, Chomaz & Billant 2012). Similar bumps in the quadratic, cubic, and quartic parts of the potential enstrophy spectra are observed here. KH instabilities on sheared layers in stratified turbulence often appear locally two-dimensional, at least early on in their evolution (Laval *et al.* 2003; Brethouwer *et al.* 2007; Waite 2011). Such flow structures would not have PV (neglecting possible viscous generation), and hence would not contribute to the total potential enstrophy. However, the horizontal vorticity of such instabilities could readily tilt into the vertical, resulting in bumps in the V_2 spectra but not V, as is observed. It would be interesting to investigate whether the bumps in the V_2 spectra change for large Re_b; the results shown here suggest that they may become more pronounced for $Re_b \gg 1$. However, this parameter regime requires very large $Re \gg 1/Fr_h^2$, and will present a serious computational challenge for some time.

On the other hand, the potential enstrophy *is* predominantly quadratic when $Re_b < 0.4$, i.e. when Fr_h is small but Re is not too large. This parameter regime corresponds to viscously coupled stratified turbulence, which is characterized by thin layers of horizontal flow, glued together by the vertical part of the viscosity. There is no small-scale turbulence in such flows; instead, the nonlinear transfer is dominated by the vertical layering, which sends energy from large to small vertical scales (e.g. Waite & Bartello 2004; Brethouwer *et al.* 2007). It is likely that the simulations of Aluie & Kurien (2011) are in this viscously coupled regime, as they have comparable numerical resolution but even stronger stratification than we do. Although their use of hyperviscosity makes it difficult to estimate Re_b, their finding that $V \approx V_2$ is consistent with our results at small Re_b. The analysis of Kurien *et al.* (2006) also applies to the small-Re_b regime, since it assumes $Fr_h \to 0$ at fixed Re. While this regime is interesting theoretically and relevant to some laboratory-scale flows (e.g. Praud *et al.* 2005), it may not apply to stratified turbulence at scales of the atmospheric mesoscale and oceanic sub-mesoscale, where Re_b is expected to be large. Thus, it is doubtful whether the assumption of quadratic potential enstrophy, and any associated cascade theory, would be applicable to stratified turbulence at such scales.

Acknowledgements

This paper benefited from comments by F. Poulin and M. Stastna. Financial support for this work was provided by the Natural Sciences and Engineering Research Council of Canada. Computations were performed on the GPC supercomputer at the SciNet HPC Consortium. SciNet is funded by the Canada Foundation for Innovation under the auspices of Compute Canada, the Government of Ontario, Ontario Research Fund – Research Excellence, and the University of Toronto.

References

ALMALKIE, S. & DEBRUYNKOPS, S. M. 2012 Kinetic energy dynamics in forced, horizontally homogeneous and isotropic, stably stratified turbulence. *J. Turbul.* **13**, N29.

ALUIE, H. & KURIEN, S. 2011 Joint downscale fluxes of energy and potential enstrophy in rotating stratified Boussinesq flows. *Eur. Phys. Lett.* **96**, 44006.

AUGIER, P., CHOMAZ, J.-M. & BILLANT, P. 2012 Spectral analysis of the transition to turbulence from a dipole in stratified fluids. *J. Fluid Mech.* **713**, 167–188.

BARTELLO, P. 1995 Geostrophic adjustment and inverse cascades in rotating stratified turbulence. *J. Atmos. Sci.* **52**, 4410–4428.

BILLANT, P. & CHOMAZ, J.-M. 2001 Self-similarity of strongly stratified inviscid flows. *Phys. Fluids* **13**, 1645–1651.

BRETHOUWER, G., BILLANT, P., LINDBORG, E. & CHOMAZ, J.-M. 2007 Scaling analysis and simulation of strongly stratified turbulent flows. *J. Fluid Mech.* **585**, 343–368.

CHARNEY, J. G. 1971 Geostrophic turbulence. *J. Atmos. Sci.* **28**, 1087–1095.

DEWAN, E. M. 1997 Saturated-cascade similitude theory of gravity wave spectra. *J. Geophys. Res.* **102**, 29799–29817.

FJØRTOFT, R. 1953 On the changes in the spectral distribution of kinetic energy for two-dimensional non-divergent flow. *Tellus* **5**, 225–230.

GODOY-DIANA, R., CHOMAZ, J.-M. & BILLANT, P. 2004 Vertical length scale selection for pancake vortices in strongly stratified viscous fluids. *J. Fluid Mech.* **504**, 229–238.

HEBERT, D. A. & DEBRUYNKOPS, S. M. 2006 Relationship between vertical shear rate and kinetic energy dissipation rate in stably stratified flows. *Geophys. Res. Lett.* **33**, L06602.

HERRING, J. R., KERR, R. M. & ROTUNNO, R. 1994 Ertel's potential vorticity in unstratified turbulence. *J. Atmos. Sci.* **51**, 35–47.

KIMURA, Y. & HERRING, J. R. 2012 Energy spectra of stably stratified turbulence. *J. Fluid Mech.* **698**, 19–50.

KURIEN, S., SMITH, L. & WINGATE, B. 2006 On the two-point correlation of potential vorticity in rotating and stratified turbulence. *J. Fluid Mech.* **555**, 131–140.

LAVAL, J.-P., MCWILLIAMS, J. C. & DUBRULLE, B. 2003 Forced stratified turbulence: Successive transitions with Reynolds number. *Phys. Rev.* E **68**, 036308.

LINDBORG, E. 2006 The energy cascade in a strongly stratified fluid. *J. Fluid Mech.* **550**, 207–242.

MOUM, J. N. 1996 Energy-containing scales of turbulence in the ocean thermocline. *J. Geophys. Res.* **101**, 14095–14109.

PEDLOSKY, J. 1987 *Geophysical Fluid Dynamics*, 2nd edn. Springer.

PRAUD, O., FINCHAM, A. M. & SOMMERIA, J. 2005 Decaying grid turbulence in a strongly stratified fluid. *J. Fluid Mech.* **522**, 1–33.

RILEY, J. J. & DEBRUYNKOPS, S. M. 2003 Dynamics of turbulence strongly influenced by buoyancy. *Phys. Fluids* **15**, 2047–2059.

RILEY, J. J. & LELONG, M.-P. 2000 Fluid motions in the presence of strong stable stratification. *Annu. Rev. Fluid Mech.* **32**, 613–657.

SMITH, L. M. & WALEFFE, F. 2002 Generation of slow large-scales in forced rotating stratified turbulence. *J. Fluid Mech.* **451**, 145–168.

WAITE, M. L. 2011 Stratified turbulence at the buoyancy scale. *Phys. Fluids* **23**, 066602.

WAITE, M. L. 2013 Direct numerical simulations of laboratory-scale stratified turbulence. In *Modelling Atmospheric and Oceanic Flows: Insights from Laboratory Experiments* (ed. T. von Larcher & P. D. Williams). American Geophysical Union (in press).

WAITE, M. L. & BARTELLO, P. 2004 Stratified turbulence dominated by vortical motion. *J. Fluid Mech.* **517**, 281–308.

WAITE, M. L. & BARTELLO, P. 2006 The transition from geostrophic to stratified turbulence. *J. Fluid Mech.* **568**, 89–108.